European Journal of Pharmaceutical Sciences 213 (2025) 107222

Contents lists available at ScienceDirect

European Journal of Pharmaceutical Sciences

journal homepage: www.elsevier.com/locate/ejps

Engineered carbon dots for mucosal gene delivery

Samuel Arca , Françoise Pons , Luc Lebeau *

Laboratoire de Chémo-Biologie Synthétique et Thérapeutique, UMR 7199 CNRS-Université de Strasbourg, Faculté de Pharmacie, 74 route du Rhin 67400 Illkirch, France

A R T I C L E I N F O

Keywords:
Carbon dots
Lung gene therapy
Mucus
Transfection
Mucopenetration
Mucolytic

A B S T R A C T

Although lung gene therapy holds promise for treating various life-threatening lung diseases, its efficacy is hindered by the mucus layer covering the airways, whose role is to protect the lung epithelium from airborne threats. For efficient gene delivery to the epithelial cells, it is necessary to ensure rapid passage of the transfection particles through the mucus layer before they are eliminated by mucociliary clearance. We developed mucus-penetrating gene carriers using carbon dots (CDs) synthesized from citric acid and bPEI600. Various strategies were investigated to convert these CDs into muco-inert nanoparticles, including PEGylation and decoration with zwitterionic or mucolytic species. After thorough characterization, we assessed their interactions with a mucus model through turbidimetry and transport measurements, as well as their effects on mucus rheology. The efficacy of the carriers to deliver DNA to various cell models was established. Particularly, Calu-3 cells, cultured at the air-liquid interface to obtain abundant mucus production, were used as a discriminating model to evaluate the potency of CDs to deliver their DNA cargo through mucus. While zwitterion-coated CDs failed to induce significant transgene expression, those with PEG decorations yielded moderate results, and CDs designed as thiol reservoirs for local mucolytic action achieved high transfection rates.

1. Introduction

According to the World Health Organization (WHO), in 2021, lung diseases (COVID-19, chronic obstructive pulmonary disease-COPD, lower respiratory infections, trachea, bronchus, and lung cancers) accounted for >18 million deaths, *i.e.* 26 % of the total 68 million deaths worldwide. (World Health Organization 2024) They ranked second after cardiovascular disorders (ischemic heart disease, stroke) in terms of mortality, incidence, prevalence, and costs. In addition, for some of these lung pathologies and many others, there is still an urgent and unmet need for effective therapeutic tools to control the disease. Since the pathophysiology of a wide range of acute and chronic lung diseases may be linked to genetic aberrations, gene therapy has rapidly become a promising strategy for their treatment and is a source of great hope for those patients with such disorders.

The lung can be used as an ideal target for local administration of a therapeutic agent owing to its unique anatomical and physiological characteristics. Pulmonary delivery is a non-invasive route of administration that targets the delivered dose directly to the site of drug action, with a possibility for self-administration improving the patient compliance. (Luo et al., 2021) It by-passes first path metabolism that is observed in oral administration and the lung has a low drug metabolizing environment. (Agu et al., 2001; Gill et al., 2007) The respiratory system offers a large surface area (100–140 m^2 (Luo et al., 2021) in humans), with thin alveolar epithelium providing a favorable environment for the topical delivery of drugs. (Forest and Pourchez, 2022) Furthermore, due to shortening of the delivery path, airway administration allows delivery of high concentration of drug to the target site with a rapid onset of action and, consequently, allows dose reduction. (Rau, 2005) Finally, the systemic drug concentration is reduced and other organs are little exposed to the drug, thus minimizing side effects. (Guo et al., 2021; Mansour et al., 2009; Sibum et al., 2018)

Although local administration of therapeutic agents to the lung has several advantages, it also has a major drawback. Indeed, absorption through the lung epithelium requires molecules to pass through a protective mucus gel layer. (Fahy and Dickey, 2010; Taherali et al., 2018) Mucus is a viscoelastic adherent secretion that is synthesized by specialized goblet and mucous cells in the epithelia that line the lumen of all of the organs and glands that are exposed to and communicate with the external environment. It is a complex hydrogel composed primarily of water (~95 %), glycoproteins (mucins, ~2–5 %), lipids, DNA, non-mucin proteins (including actin), and cell debris. (Bansil and Turner, 2018) Mucins are the major functional components of mucus and are responsible for the essential and predominant viscoelastic

* Corresponding author.
E-mail address: llebeau@unistra.fr (L. Lebeau).

https://doi.org/10.1016/j.ejps.2025.107222
Received 10 February 2025; Received in revised form 25 July 2025; Accepted 30 July 2025
Available online 30 July 2025
0928-0987/© 2025 The Authors. Published by Elsevier B.V. This is an open access article under the CC BY license (http://creativecommons.org/licenses/by/4.0/).

properties of the mucus layer. They are exceedingly large proteins (up to 3×10^6 Da per monomer) and consist of approximately 50–80 % (w/w) carbohydrates assembled in oligosaccharide chains of 2-20 saccharide units, in both linear and moderately branched structures. Most mucin glycoproteins have terminal cysteine-rich domains that can form disulfide bridges, and a high sialic acid and sulfate content, which leads to a strongly negative surface that increases the rigidity of the polymer *via* charge repulsions. (Shogren et al., 1989) Two of these mucins, MUC5AC and MUC5B, are strongly expressed in the airways and gastro-intestinal tract. (Rose and Voynow, 2006; Thornton et al., 2008) The mucus structure does primarily result of entangled mucins and other mucus constituents with more or less linear structure, like DNA and actin filaments, that essentially originate from debris of shed epithelial cells and neutrophils. (Broughton-Head et al., 2007; Matthews et al., 1963) In addition to physical entanglement, low-affinity non-covalent bonds and stronger disulfide bonds between mucin fibers create a three-dimensional mesh-like network which imparts mucus its particular viscoelastic trait. Armed with these properties, mucus has critical functions in protecting mucosal tissues from attack by pathogens and toxins, while permitting diffusion, exchange and absorption of gases (lung and eye) and nutrients (gastrointestinal tract) with the underlying epithelium. It thus acts as a barrier with selective permeability to molecules, foreign particles and pathogens that enter the hydrogel matrix. (Witten et al., 2018) First, mucus performs as a steric filtering barrier for particles larger than the mesh-spacing or pore-size of the mucin network. Second, due to its complex chemical composition, mucus can also slow down the diffusion of smaller particles and molecules through electrostatic or hydrophobic interactions. (Cone, 2009; Lieleg and Ribbeck, 2011) Third, in the lung, polymeric mucins are continuously synthesized and secreted, and the mucus gel is propelled in a proximal direction by ciliary beating, clearing inhaled particles, pathogens, and dissolved chemicals that can damage the pulmonary tissue. (Knowles and Boucher, 2002) Besides, most pulmonary obstructive disorders are associated with chronic inflammation, leading to hypersecretion and possibly lower hydration of mucus in the airways which forms an even more effective barrier against inhaled therapeutic agents.

Mucus lining the airway epithelium has thus been recognized as one of the greatest obstacles to overcome for promoting efficient lung gene transfer as it readily traps transfection particles (*i.e.,* nanocarrier-associated nucleic acid) that are rapidly eliminated from the lung by mucociliary clearance mechanism, before they can diffuse and reach the underlying target epithelial cells. (Kim et al., 2016; Kolb et al., 2006; Pickles, 2004) To address the critical challenge of nanomedicine delivery to mucosal tissues, various strategies have been deployed for enhancing their penetration through the mucus layer. They include the use of muco-adhesive or muco-inert (muco-penetrating) materials, of agents that regulate mucus secretion, of mucolytic agents that may disrupt the mucus barrier, and of absorption enhancers. (Balsamo et al., 2010; Ghadiri et al., 2019; Laffleur and Bernkop-Schnurch, 2013; Watchorn et al., 2022; Wu et al., 2018) For gene delivery to the lung, essentially muco-penetrating and mucolytic approaches have been described. (Ensign et al., 2012; Lai et al., 2009) It is now well established that regardless of their size, hydrophobic (Schuster et al., 2013; Suk et al., 2009) or positively charged (Kim et al., 2013) particles cannot efficiently penetrate airway mucus. Consequently, much effort has been devoted to decoration of transfection particles with hydrophilic and neutral polyethylene glycol (PEG), and PEGylated nanoparticles (NPs) are now at the cutting edge to overcome the mucus layer. (Huckaby and Lai, 2017) However, this approach has shown some limitations since repeated administration results in production of anti-PEG antibodies that provoke extensive trapping and neutralization of mucus-penetrating PEGylated NPs. (Henry et al., 2016) Anionic polymers have been used to coat cationic transfection particles and form delivery vectors enabling mucus penetration. (Zhu et al., 2022; Zhang et al., 2024) As an other alternative to PEGylation, virus-like particles have been proposed which display high surface charge density with a neutral net charge, thus minimizing electrostatic interactions with mucins through a rapid exchange mechanism. (Schattling et al., 2017) This strategy of "slippery" NPs has been initially proposed for the delivery of drugs (Laffleur et al., 2014) but had proved successful as well for nucleic acid delivery. (Li et al., 2015; Peng et al., 2020; Sun et al., 2013) With regard to mucolytic approaches, they essentially consist in pretreatment of the airways with mucolytic agents (*N*-acetyl cysteine, nacystelyn). (Ferrari et al., 2001; Kushwah et al., 2007; Suk et al., 2011) Mucolytics are compounds with sulfhydryl groups that are able to dissociate disulfide bonds reticulating mucins, releasing strains in the biopolymer and potentially reducing mucus viscosity. Other compounds, such as proteolytic enzymes, are able to decrease elastic properties and dynamic viscosity of mucus by cleaving amide bonds within amino acid sequence of mucins. (Majima et al., 1988) Recombinant human deoxyribonuclease (rhDNase) is not strictly mucolytic since its mechanism of action is not based on breaking up mucus, but on degradation of neutrophil-derived DNA entangled with mucin bundles. (Dasgupta and King, 1996) To the best of our knowledge, the use of proteolytic enzymes has not yet been described for gene transfer to airway epithelium, while that of rhDNase is not consistent with the preservation of the transgene structural integrity. These protocols and mucoactive gene carriers are used primarily to enhance the efficiency of non-invasive gene delivery to mucosal tissues where “traditional” carriers may be impeded by the mucus barrier. The potential main indications include respiratory diseases (*e.g.*, cystic fibrosis-CF, to deliver genes that correct CFTR mutations directly to airway epithelial cells, chronic obstructive pulmonary disease-COPD, for genes targeting airway remodeling and inflammation, lung cancer…), but also gastrointestinal disorders (*e.g.*, inflammatory bowel disease, gastrointestinal cancer, and gastroesophageal reflux disease), reproductive tract infections or other conditions (vaginal or cervical gene therapy), and ocular diseases (*e.g.*, age-related macular degeneration-AMD, glaucoma). A most recent indication refers to intranasal mRNA vaccination.

The aim of this study was the development of novel mucus permeating nanocarriers for gene delivery to mucosal tissue, based on carbon dots (CDs). CDs are carbonaceous quantum dots that combine several favorable attributes of semiconductor-based quantum dots (nanoscale size, size- and wavelength-dependent luminescence emission, resistance to photobleaching, ease of bioconjugation), but with no or low associated toxicity, and not requiring tedious or costly preparation steps. (Kaurav et al., 2023; Lim et al., 2015; Mansuriya and Altintas, 2021) Immediately upon their discovery in 2004, (Xu et al., 2004) CDs have been subject of a number of studies as potential drug delivery agents, and more recently as nucleic acid carriers. (Biswal and Bhatia, 2021; Othman et al., 2024; Yazdani et al., 2024) As a matter of fact, these NPs can be conveniently decorated with polyamines, especially polyethyleneimine (PEI) which is a potent gene delivery reagent. (Neuberg and Kichler, 2014) Consequently, they may display nucleic acid condensation properties as is required for intracellular delivery of genetic material. We thus prepared CDs from citric acid and low molecular weight branched PEI (bPEI600, MW = 600 Da) as a NP platform and decorated their surface with ten different types of grafts, PEG, zwitterions, and thioesters, in order to obtain mucus penetrating properties. The physical and chemical properties of the grafted NPs, including grafting ratio, particle dimension, surface potential, and density of charge were determined using nuclear magnetic resonance (^{1}H-NMR) and dynamic light scattering (DLS). We conducted a NP-mucus interaction study that included turbidimetric and rheological measurements, and permeation assays to evaluate the mucus penetrability of the NPs. Finally, the capacity of the carriers to condense plasmid DNA (pDNA) and promote transfection in various cell models, in the absence or presence of a protective mucus layer has been determined. The results of our study should therefore provide a more thorough understanding of the behavior of CDs and related CD/DNA complexes, hereinafter referred to as dotoplexes, in mucosal environment with prospects for gene delivery to the lung.

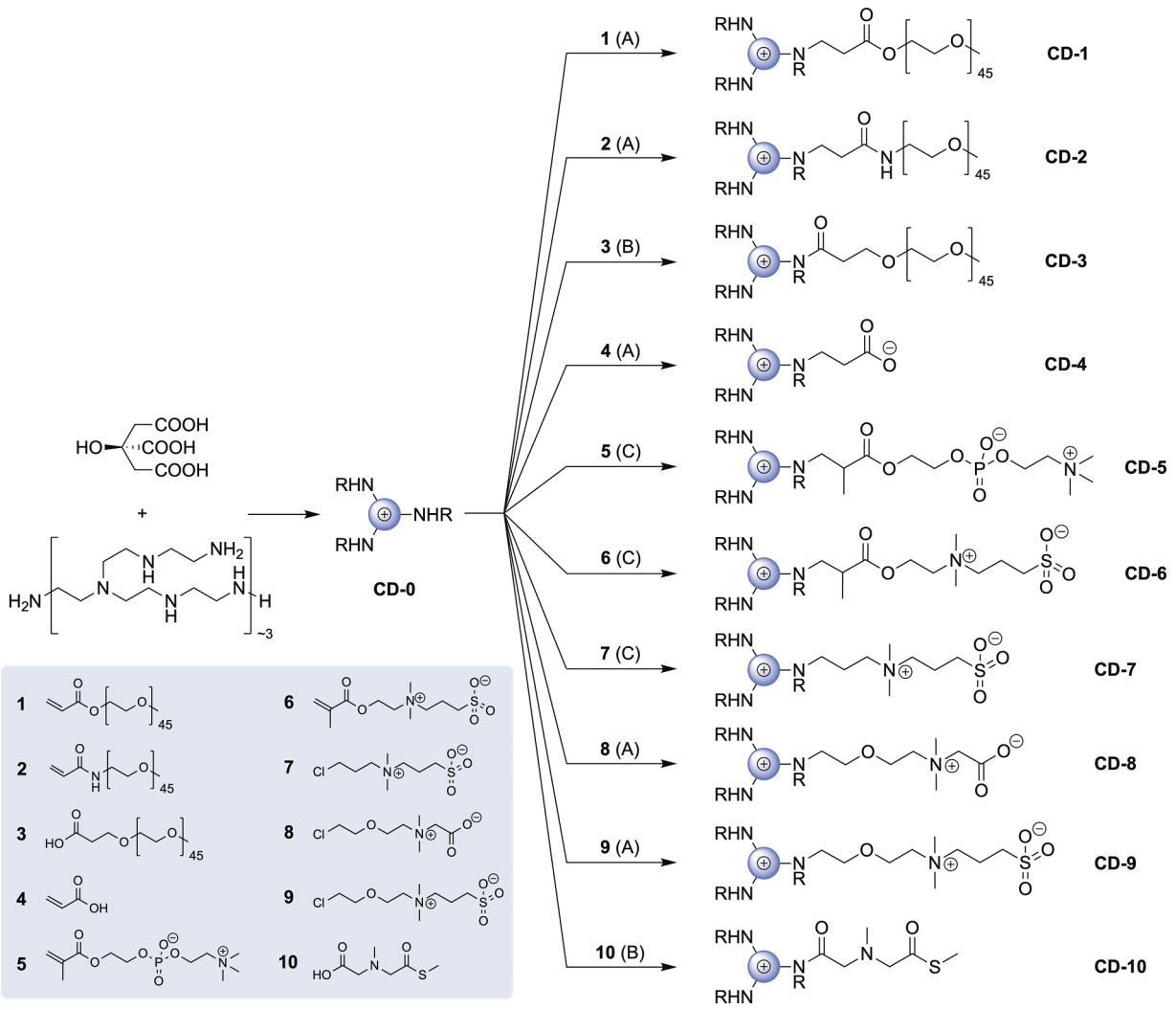

Fig. 1. Synthetic route to the mucoactive CDs. Parent nanoparticle **CD-0** was derivatized with reagents **1**–**10**, according to the general protocol (A, B, C) indicated into brackets (for experimental details, see Supporting Information).

2. Experimental sections

2.1. Materials and methods

Citric acid, bPEI25k, bPEI600, poly(ethylene glycol) monomethyl ether MW 2000 Da (mPEG2000), acrylic acid (**4**), 2-methacryloyloxyethyl phosphorylcholine (**5**), sulfobetaine methacrylate (**6**), propane sultone, poly(acrylic acid) (PAA, MW 1800 Da), 3-(dimethylamino) propyl chloride hydrochloride, bis(2-chloroethyl) ether, 3-(4,5-dimethylthiazol-2-yl)-2,5-diphenyl tetrazolium bromide (MTT), DNA from calf thymus, and type III mucin from porcine stomach (PGM) were from Sigma-Aldrich (St Louis, MO, USA). They were used as received. Coelenterazine was from Alfa Aesar (Biesheim, France). Dialysis membranes were from Spectrum Laboratories (Rancho Dominguez, CA, USA). A549 (human lung carcinoma; CCL-185) and Calu-3 cells (human epithelial adenocarcinoma; HTB-55) were obtained from ATCC-LGC (Molsheim, France). Plasmid pCMV-GLuc (5.7 kbp) was from Nanolight Technology (Pinetop, Az, USA), pDNA concentration refers to phosphate content. Fetal bovine serum (FBS), culture media (Dulbecco's Modified Eagle Medium, DMEM) and supplements were from GIBCO-BRL (Cergy-Pontoise, France).

NMR spectra were recorded on a Bruker 400 MHz Avance III instrument. Chemical shifts δ are reported in ppm relative to solvent residual peak in $CDCl_3$ (^{1}H: $CHCl_3$ at 7.27 ppm; ^{13}C: $CDCl_3$ at 77.0 ppm), or to an internal reference in D_2O (^{1}H: *t*-BuOH at 1.24 ppm, ^{13}C: *t*-BuOH at 70.4 and 30.3 ppm).

All CDs and buffer solutions were prepared with deionized water purified with an EMD Millipore Milli-Q™ integral system (resistivity ≤ 18.2 MΩ.cm) and filtered through a 0.22 μm polyethersulfone (PES) membrane (Millex).

2.2. Synthesis of the parent nanoparticle *CD-0*

In a 50 mL borosilicate reaction flask, citric acid (2.0 g), bPEI600 (8.0 g) and water (20 mL) were mixed under vigorous stirring to form a homogenous solution. The mixture was then heated to 220 °C in the open air to remove water (*ca.* 15 mL) until it formed a viscous sirup. Then the reaction vessel was fitted with a reflux condenser and stirred for 6 h at this temperature. The resulting dark-brown sticky residue was dissolved in ultrapure water and brought to pH 7.4 with conc. HCl. The solution was transferred into a dialysis bag (Spectra/Por 3, MWCO 1000 Da) and equilibrated for 72 h against water, with periodical replacement of the dialysate. The resulting brown-yellow solution was then filtered through a 0.22 μm PES membrane and freeze-dried at -50 °C for 24–36 h to yield **CD-0** (*ca.* 0.75 g).

2.3. Post-functionalization of CD-0

CD-1 to **CD-10** were all obtained starting from the same precursor **CD-0** that was reacted with compounds **1** to **10** under various experimental conditions, using general protocols A, B or C (Fig. 1). Reagents were commercially available (**4**–**6**) or prepared in the laboratory (cf. Supporting Information for detailed synthesis).

Protocol A. A solution of **CD-0** (400 mg) in ultrapure water (5 mL) was adjusted at pH 8.5 before reactive acrylate **1** (200 mg) was added. The reaction mixture was stirred for 7 d at rt. Purification was performed through lavage of the aqueous solution with $CHCl_3$ (3 × 5 mL), filtration (0.22 μm), and freeze drying. **CD-1** (74 mg) was obtained as a light-yellow hygroscopic powder.

CD-2 (99 mg), **CD-4** (39 mg), **CD-8** (18 mg), and **CD-9** (29 mg) were obtained according to the same protocol (except for the purification step), starting from **CD-0** (100 mg) and acrylamide **2** (10 mg), acrylic acid **4** (100 mg), or alkyl halides **8** (100 mg) or **9** (100 mg). **CD-2, CD-4, CD-8**, and **CD-9** were purified by dialysis (MWCO 1000 Da) against water for 48 h, filtered (0.22 μm), and freeze-dried.

Protocol B. In a solution of **CD-0** (100 mg) in ultrapure water (5 mL) at pH 6.0 were sequentially added carboxylic acid **3** (200 mg, 0.09 mmol), EDC.HCl (37 mg, 0.19 mmol), and sulfo-NHS (41 mg, 0.19 mmol). The reaction mixture was stirred for 7 d at rt. It was purified by dialysis (MWCO 1000 Da) against water for 48 h, filtered (0.22 μm), and freeze dried to yield **CD-3** (36 mg) as a light-orange hygroscopic powder.

CD-10 (87 mg) was obtained as a light-yellow hygroscopic powder according to the same protocol, from **CD-0** (100 mg), carboxylic acid **10** (50 mg, 0.28 mmol), EDC.HCl (108 mg, 0.56 mmol), and sulfo-NHS (61 mg, 0.56 mmol).

Protocol C. A solution of **CD-0** (100 mg) in ultrapure water (5 mL) was adjusted at pH 9.0 with aqueous NaOH. It was then evaporated under reduced pressure and co-evaporated three times with anhydrous DMF (5 mL). The yellow residue was suspended in DMF (5 mL), methacrylate **5** (100 mg) was added, and the suspension was stirred at 75 °C for 5 d. It was then reduced under vacuum and the residue was purified by dialysis (MWCO 1000 Da) against water for 48 h, filtered (0.22 μm) and freeze-dried to yield **CD-5** (74 mg) as a light-yellow hygroscopic powder.

CD-6 (32 mg) and **CD-7** (18 mg) were obtained similarly, from **CD-0** (100 mg) and reagents **6** (100 mg) and **7** (100 mg), upon heating for 3 d at 100 °C and 75 °C, respectively.

2.4. Nanoparticle characterization

Whenever possible, functionalization ratio was determined by ^{1}H NMR measurements. In brief, ^{1}H-NMR spectrum was recorded from a mixture of **CD-0** and the grafting reagent (5.0 mg of each) in D_2O. From ^{1}H-NMR spectra obtained for the grafted NPs, the amount of decorations (in mmol/g) was calculated by simple application of the rule of three, considering two specific NMR signals that were preserved upon conjugation, one being characteristic of **CD-0**, and the second of the grafting reagent. Optical and photoluminescence properties of CDs were determined by recording UV–visible and fluorescence spectra of CD preparations (pH 7.4), using a multimode reader (Varioskan Lux, Thermo Fisher Scientific, France). The hydrodynamic diameter and zeta (ζ) potential of the NPs were measured by dynamic light scattering (DLS) and electrophoretic light scattering (ELS), respectively, using a Zetasizer NanoZS apparatus (Malvern Instruments, Paris, France). All measurements were performed in triplicate on samples (1 mg/mL) in 1.5 mM NaCl, pH 7.4, at 25 °C. Data were analyzed using the multimodal intensity distribution software supplied with the instrument and expressed as mean (± SD). Density of surface charge (electrokinetic charge, Q_{ek}) was determined by polyelectrolyte titration with PAA, according to a previously published procedure. (Weiss et al., 2021) Briefly, evolution of ζ-potential of a solution of CDs (1.0 mL at 1.0 mg/mL in NaCl 1.5 mM, pH 7.4) along spiking with a solution of PAA (10.0 mg/mL in NaCl 1.5 mM, pH 7.4) was recorded. Q_{ek} was calculated from the amount of PAA (mmol of acrylic acid units) required for reversing the sign of ζ-potential (isoelectric point), as determined by interpolation of the titration curve. Q_{ek} is expressed in mmol/g.

2.5. Preparation of CD/pDNA complexes

The CD/pDNA complexes were prepared at various weight ratios by mixing equal volumes of CDs and pDNA solutions (prepared at the adequate concentration in ultrapure water). The dotoplexes were allowed to form for 30 min at rt without handling. Finally, the mixture was homogenized by pipetting up and down and subsequently used for agarose gel electrophoresis and transfection experiments. bPEI25k/pDNA complexes were prepared similarly, from a bPEI25k solution at adequate concentration.

2.6. pDNA complexation assay

Complexation of pDNA by CDs was investigated using a nucleic acid retardation assay. For this, freshly prepared dotoplexes (20 μL, containing 0.8 μg pDNA) were mixed with loading buffer (2 μL, Invitrogen), and the mixtures were deposited in the wells of a 1 % agarose gel prepared in TAE buffer (40 nM Tris base, 20 mM acetic acid, 1 mM EDTA). "Naked" DNA (0.8 μg in 20 μL) supplemented with loading buffer (2 μL) was deposited in a well as a control. The gel was then subjected to an electric field of 100 V, in TAE buffer, for 60 min. DNA was stained by soaking the gel in an ethidium bromide solution (0.5 μg/mL, QBiogene) for 15 min. The gel was then washed in a bath of ultrapure water and imaged under UV light using a gel imager (Amersham Imager, GE Healthcare).

2.7. Turbidimetric measurements

The interaction between CDs or the dotoplexes made thereof and mucin fibers was investigated by turbidimetry. (Porsio et al., 2018) For that, a solution of PGM (40 mg/mL, 50 μL) in PBS pH 7.4 was mixed with an aqueous solution of CDs (10 mg/mL, 200 μL) or dotoplexes (200 μL, obtained after complexation of the same amount of CDs with DNA from calf thymus) in ultrapure water. Solutions containing PGM, CDs or dotoplexes alone were prepared in parallel to serve as controls. The samples (100 μL) were then deposited into 96-well plates and submitted to gentle orbital shaking at 37 °C for 1 h. At the end of the incubation period, ability of the solutions to scatter light (λ = 600 nm) was quantified using a plate reader (Varioskan Lux, Thermo Scientific). Experiments were run in triplicate, and results were expressed as relative absorbance (ΔA) according to the eq (1):

$$\Delta A = A_S - A_{CD} - A_{PGM} - A_{PBS} \quad (1)$$

where A_s, A_{CD}, A_{PGM}, and A_{PBS} stand for the absorbances measured with the sample, the solution of CDs or dotoplexes alone, the solution of PGM alone, and PBS alone, respectively.

2.8. Mucopenetration measurements

The ability of CDs and dotoplexes to penetrate an artificial mucus layer was investigated using 24-well Transwell® plates. These experiments were realized in a humidified chamber to avoid drying effects that could superimpose the actual transport phenomena. In brief, a mucus layer was created by evenly depositing 25 μL of a PGM solution (30 mg/mL in PBS) on the membrane of an insert (Falcon®: PET membrane, surface area of 0.33 cm^2, pore size of 0.4 μm). The semipermeable membrane allows for the passage of small molecules but retain the mucin hydrogel in the insert. The insert was then placed in the well of a 24-well culture plate containing 700 μL of PBS, with the insert acting as the donor compartment and the well of the plate acting as the acceptor

compartment. After 30 min incubation at 37 °C to allow the mucus layer to equilibrate, a solution of CDs (12.5 μL at 10 mg/mL in ultrapure water) or of dotoplexes prepared with calf thymus DNA (12.5 μL at 10 mg/mL in ultrapure water) was carefully deposited onto the mucus layer. At the same time, the same amount of CD or dotoplex solution to be tested was deposited into an insert containing PBS (25 μL) in place of mucus (control condition). After incubation at 37 °C for 5 h, the contents of each basolateral compartment was recovered (700 μL) and placed overnight in an incubator at 60 °C to obtain a dry pellet. The pellets were resuspended in ultrapure water (110 μL), and the amount of CDs or dotoplexes present in the resulting solutions was quantified by measuring fluorescence intensity using excitation and emission wavelengths at 370 and 460 nm, respectively (Varioskan Lux multimode reader, Thermo Scientific). Translocation efficiency of the NPs through the mucus layer was expressed as percentage by dividing the fluorescence intensity measured for each insert with mucus by the fluorescence intensity measured for the corresponding insert without mucus (control).

2.9. Rheological measurements

To assess if addition of CDs or the corresponding dotoplexes to a mucin hydrogel induces electrostatic cross-linking of the mucin filaments in the gel matrix, oscillatory shear rheology measurements were realized on a Haake Mars 60 instrument equipped with a 25 mm diameter parallel-plate setup (Thermo Electron, Karlsruhe, Germany). We determined the viscoelastic properties of mucin hydrogel either in the absence or in the presence of CDs. The mucin samples without CDs were obtained by solubilizing PGM lyophilizate in PBS (100 mg/mL) and adjusting pH to 7.4 with NaOH. Mucin samples containing CDs were prepared by solubilizing PGM lyophilizate (100 mg) in ultrapure water (1 mL) containing CDs (5 mg/mL). The resulting mixtures were subjected to rotational stirring at rt until complete dissolution and homogeneity, and pH was brought to 7.4. The plates of the rheometer were equilibrated at 20 °C for 2 min, before sample deposition (180 μL). After another 2 min equilibration period, oscillatory measurements were performed at 20 °C, using a 3 mm gap width between the two plates. The linear viscoelasticity (LVE) domain of each sample, *i.e.* where the viscoelastic characteristics of mucus were preserved, was first determined by performing a strain amplitude sweep (γ: 0.0001-10) at a frequency of 1 Hz. This measurement allowed defining the strain amplitude to be used when measuring the storage (elastic, G') and loss (viscous, G") moduli. This is crucial for probing the microstructure of the mucin gel at equilibrium to gently stress but not disrupt the gel cross-links and entanglements. The frequency dependence of the G′ and G" moduli were calculated from the measured response of the sample to the oscillating angular displacement. All the frequency sweep data were collected at a strain amplitude of 0.05 and between 0.0178 and 1.78 Hz.

2.10. Cell culture

The lung epithelial cells A549 and Calu-3 were cultured in complete DMEM/F12 culture medium, *i.e.* containing 10 % FBS (Fetal Bovine Serum), 100 U/mL penicillin, 100 μg/mL streptomycin, 5 mM HEPES and 2 mM L-glutamine. Cultures were grown in 75 cm^2 culture flasks at 37 °C in a 5 % CO_2 humidified chamber. At 80-100 % confluency, cells were detached from the flasks by trypsin treatment (0.05 % trypsin-EDTA in PBS) and then seeded either in new flasks to maintain the culture, or in 96-well plates and/or 24-well inserts for transfection experiments. A459 and Calu-3 cells were seeded in 96-well plates at a density of 6.0×10^4 and 1.0×10^5 cells/well, respectively, in 100 μL of culture medium. Plates were used for transfection experiments 24 h after seeding. Calu-3 cells were seeded onto inserts (PET; 0.4 μm pore size) at a density of 1.0×10^5 cells/insert in 400 μL of culture medium. Three days later, the apical culture medium of the inserts was removed, and the cells were cultured at the air-liquid interface (ALI) for 7 d. During this period, the culture medium in the basolateral compartment of the inserts was replaced every 2 to 3 d. Transfection experiments were started on d 7 of ALI culture.

2.11. Transfection assay

In plate cultures, freshly prepared dotoplexes (10 μL containing 0.4 μg of pDNA) were deposited in each well containing 100 μl of culture medium and transfection efficiency was assessed 24 h later. In ALI cultures, at d 7, complete culture medium (100 μL) was added to the apical compartment of each insert, followed 1 h later by freshly prepared dotoplexes (10 μL containing 1.6 μg of plasmid DNA) and transfection efficiency was assessed 24 h or 72 h later. For the 72-h condition, dotoplexes were removed from the inserts 24 h after deposition. To do this, the supernatant was aspirated and replaced with fresh complete culture medium. In all experiments, untreated cells were used as a negative control and each condition was tested in triplicates (plate cultures) or duplicates (ALI cultures). The plasmid DNA (pCMV-GLuc) used in these experiments encodes the *Gaussia princeps* luciferase (Gluc). As Gluc is an excreted protein, transfection efficiency can be straightforwardly evaluated by directly measuring luciferase activity in the culture supernatant. To do this, a solution of coelenterazine (1.5 μM, 50 μL), a substrate of Gluc, was added to an aliquot of culture supernatant (20 μL) and the resulting bioluminescence was measured over a 1-second period (Varioskan Lux, Thermo Scientific). Transfection efficiency was expressed in relative luminescence units (RLU).

2.12. Cytotoxicity assay

Parallel to transfection assays, mitochondrial activity was measured using an MTT colorimetric assay, in order to quantify cell viability and thus assess cytotoxicity of the CD/DNA complexes. At the end of cell treatment (24 or 72 h), culture medium was removed and cells were carefully washed with PBS. Complete culture medium containing MTT (1.0 mg/mL) was added to the cells (100 μL/well) that were incubated for 1 h at 37 °C. Then culture medium was removed again and DMSO (100 μL) was added to lyse cells and dissolve reduced MTT (formazan) produced by the mitochondrial succinate dehydrogenase. Intensity of MTT reduction was then evaluated by measuring absorbance of the resulting solution at 570 nm with a correction at 690 nm. Cell viability was expressed as the percentage of the absorbance of dotoplex-treated cells relative to that of untreated cells. Value for each sample is the mean of triplicate determinations.

2.13. Statistical analysis

Data were expressed as mean ± SD. Statistical differences between groups were determined by a Student's *t*-test using the Kaleidagraph 5.0.6 software. Data were considered as significantly different when p value was <0.05.

3. Results and discussion

3.1. Preparation and characterization of CDs

First, we synthesized cationic **CD-0** as a reference and to serve as a platform for grafting with the various decoration species (Fig. 1). Briefly, citric acid and bPEI600 (1/4, w/w) were heated in open air at 220 °C for 6 h in the minimum amount of water (see Supporting Information for complete description). The resulting **CD-0** was purified by dialysis and was obtained in *ca.* 7.5 %. Though bPEI25k is most often used to construct CDs for transfection purpose, low molecular weight bPEI600 was preferred because non reacted materiel can be efficiently separated from NPs by dialysis, which is definitely not the case with the higher molecular weight polymer bPEI25k. (Claudel et al., 2019; Pierrat et al., 2015)

Table 1
Physical and photophysical characteristics of **CD-0** to **CD-10**.

NPs	Size (nm)	ζ-potential (mv)	Q_{ek} (mmol/g)	FR (mmol/g)	λ_{max} (nm)	λ_{ex} (nm)	λ_{em} (nm)
CD-0	10.4 ± 0.2	+22.4 ± 0.6	3.8	–	340	350	450
CD-1	105.8 ± 1.6	+29.9 ± 3.8	3.5	0.01	340	350	450
CD-2	125.1 ± 12.3	+23.9 ± 0.2	3.4	0.06	350	360	455
CD-3	23.5 ± 1.6	+5.9 ± 3.0	1.6	1.19	350	360	455
CD-4	22.5 ± 1.6	+21.6 ± 5.1	2.8	1.21	350	360	450
CD-5	23.1 ± 2.3	+6.1 ± 0.8	0.7	0.31	350	360	450
CD-6	27.3 ± 0.3	−0.7 ± 0.1	0.2	0.17	350	360	450
CD-7	18.1 ± 2.7	+31.9 ± 1.9	3.2	1.03	350	360	450
CD-8	4.9 ± 0.3	+3.3 ± 1.9	nd	1.74	350	360	450
CD-9	11.9 ± 1.2	+11.0 ± 1.1	3.1	0.42	350	360	450
CD-10	72.9 ± 4.9	+59.9 ± 6.0	2.9	nd	350	360	450

*FR: functionalization ratio. nd: not determined.

In order to equip the carriers with mucopenetrating properties, several types of particle decoration were considered. First, three different PEGylated particles were engineered to exhibit disparate biodegradability properties. They were accessed by three different ways. **CD-1** and **CD-2** were obtained *via* aza-Michael addition reaction of amines available at the surface of **CD-0** to acrylate **1** and acrylamide **2**, respectively. **CD-3** was prepared by carbodiimide coupling between **CD-0** and carboxylic acid-terminated PEG derivative **3**. In the first two cases, the net cationic charge of the NPs was preserved whereas in the case of **CD-3**, grafting of the PEG chains resulted in a loss of cationic charges due to the formation of neutral amide bonds. Due to the ester or amide bonds connecting PEG chains to these CDs, differences in the biodegradability of NPs can be expected with possible positive outcome in cell uptake or endosome escape and, ultimately in transfection efficiency.

Second, CDs displaying a high surface charge density with a neutral net charge after nucleic acid complexation were designed to obtain virus-like or slippery NPs. Six different reagents were thus used to densely coat the NPs with zwitterionic species. In order to modulate the strength of the transient mucus-transfection particle interactions, carboxy-, phospho-, and sulfo-betaines were introduced on **CD-0**. It is well documented that carboxylates, phosphates, and sulfates associate with ammonium cations to form complexes with different dissociation constants. It is hypothesized that the presence of such decorations on CDs will result in varying exchange rates with competing anions of the mucus, which will consequently have an impact on the particle diffusion rate. **CD-4** was obtained through aza-Michael reaction of amines on the platform CDs with acrylic acid **4**. In this case, the creation of zwitterionic groups, carboxybetaines, originated from the introduction of anionic carboxyl groups at the surface of the NPs and, consequently, resulted in a decrease in their net cationic charge. Aza-Michael reaction of **CD-0** with phosphobetaine and sulfobetaine methacrylates **5** and **6** afforded **CD-5** and **CD-6**, with full preservation of the cationic net charge of the NPs. Similarly, nucleophilic displacement of the chlorine atom in reagents **7, 8**, and **9**, by the amine groups distributed on **CD-0**, resulted in the introduction of zwitterionic moieties within the CDs structure, without decreasing the number of ionizable amine groups, *i.e.*, preserving the net cationic charge of the NPs.

Finally, CDs were decorated with substituents bearing a methyl thioester group. It is hypothesized that hydrolysis of the thioester, when exposed to the enzyme activity present in mucus, will generate methyl mercaptan. This, in turn, will lead to the reduction of disulfide bridges that reticulate mucins, causing an enlargement of the mucus mesh and facilitating the diffusion of the transfection particles within the biopolymer. Carboxylic acid reagent **10** was thus reacted with **CD-0** by means of a carbodiimide-mediated coupling reaction to yield **CD-10**. Though the reaction involved creation of an amide bond, loss of a cationic charge on **CD-0** was compensated for by the presence of a tertiary amine in reagent **10**.

All the NPs were thoroughly characterized (Table 1). Hydrodynamic diameters were measured by DLS, and ζ-potential and density of charge (Q_{ek}) by ELS experiments. Whenever possible, ratio of functionalization of **CD-0** with the electrophilic species **1** to **10** was determined by ^{1}H NMR measurements. The photophysical properties of the NPs were investigated using UV-vis and fluorescence spectroscopy.

The size of the NPs appears variable depending on the type of surface decoration introduced on **CD-0**. The hydrodynamic diameter of the parent particle was determined to be 10.4 ± 0.2 nm, with a ζ-potential value of +22.4 ± 0.6 mV. A significant increase in the size of the NPs was observed upon PEGylation in the case of **CD-1** and **CD-2** (105.8 ± 1.6 nm and 125.1 ± 12.3 nm, resp.), whereas ζ-potential did not change much. These size increases reveal some aggregation which was unexpected considering the high ζ-potential value of the NPs. This can be paralleled with the corresponding functionalization ratios which are low for these two CDs. The reason why scarce decoration of the NPs with PEG chains would promote aggregation is not clear. Maybe an explanation could be found in interdigitation of the PEG chains from a particle with those of neighboring ones through hydrogen bonds, dipole-dipole or hydrophobic interactions. (Uchida et al., 1956) This polymer-polymer interaction phenomenon resulting in polymer entanglement and particle aggregation would only occur at low density of PEG coating on NPs since, at high coating density, segmental flexibility of PEG produces a high degree of steric exclusion resulting in the well known stealth effect of the polymer. This hypothesis however is speculative and would deserve a more in-depth analysis. With a higher density of PEG grafting, **CD-3** shows a hydrodynamic diameter of 23.5 ± 1.6 nm and a positive surface charge which appears significantly low (ζ = +5.9 ± 3.0 mV) when compared to **CD-0**. This is a result of the transformation of part of titratable amine groups on **CD-0** into non titratable amide groups. This may also reflect some hiding of the residual cationic charges on the NPs by the densely grafted PEG chains, leading to understating their amount. This is supported by data on DNA complexation (*vide infra*). On the other hand, zwitterion-decorated NPs all display a size in the 10–20 nm range, except for **CD-8** that appears even smaller than **CD-0**. This can be explained considering CDs as core-shell structures with PEI forming a corona around the graphitic core. At pH 7.4, most amines in PEI (*ca.* 80 %) (Shepherd and Kitchener, 1956) are protonated and the electrostatic repulsions between the ammonium groups make the polymer to expand. Due to the high functionalization ratio of **CD-8** with the carboxybetaine moiety (1.74 mmol/g), the repulsions between the PEI ammonium groups distributed around the CD core are substantially mitigated by the carboxylate groups. This makes the PEI corona collapse to a certain extent and thus results in a decrease in the hydrodynamic diameter of the particles when compared to **CD-0**. As the introduction of zwitterionic decorations onto **CD-0** by means of reagents **4-9** proceeded through alkylation of amine groups on the NPs, an upwards shift of the pk_a value of the alkylated amines is expected, except in the case of amine quaternarization. In any case, these decorations should theoretically result in an increase in the concentration of ammonium species at the surface of the NPs. This may or not translate into an increase of the ζ-potential value, depending on

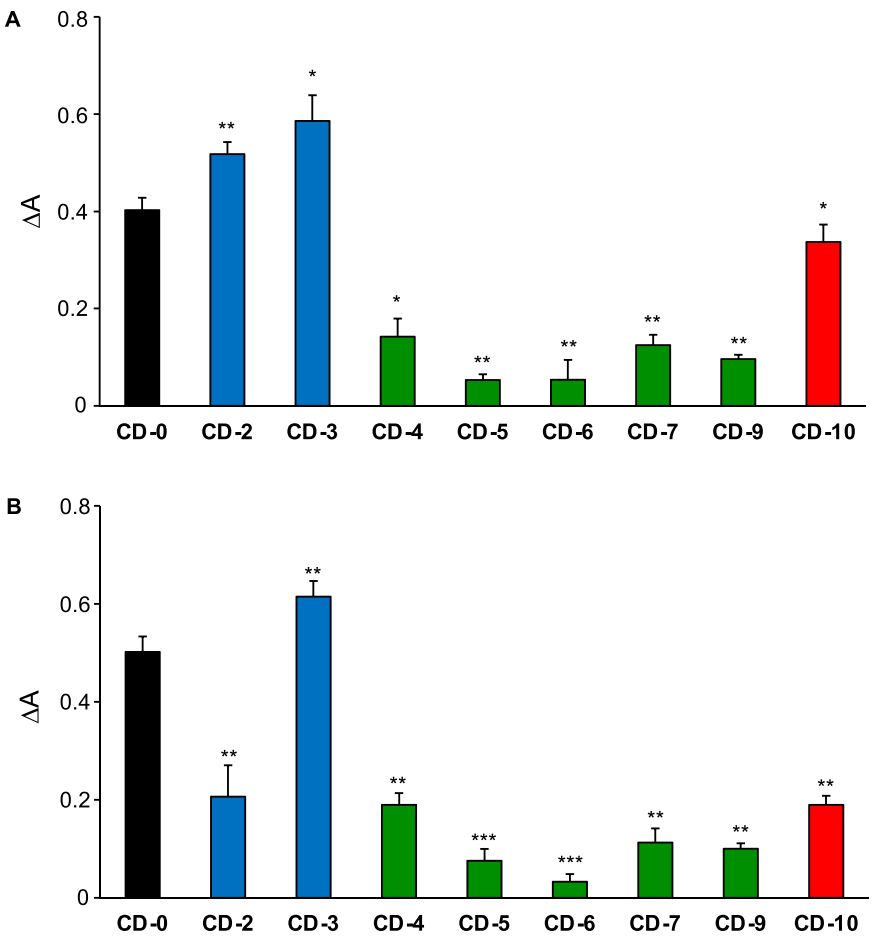

Fig. 2. (Assessment of the interactions between mucin and CDs (**A**), and CD/DNA complexes (**B**) through turbidimetric measurement. CD/DNA ratios (w/w) assayed in these experiments were those for which transfection efficiency was optimum in the Calu-3 ALI model (*vide infra*). Results are expressed as the variation of absorbance (ΔA) after mixing a mucin solution with different NPs for 1 h at 37 °C. Results are the mean ± SD of n = 3–4 experiments. Statistical differences when compared to **CD-0** were determined by Student's *t*-test: $p < 0.05$ (*), $p < 0.01$ (**), and $p < 0.001$ (***).

the spatial distribution of the cationic groups at the periphery of the NPs, internal charges less contributing to the average electrostatic potential existing at the hydrodynamic plane of shear or "slipping" plane. The highly fluctuating ζ-potential measured for **CD-4** to **CD-9** (from −0.7 to +31.9 mV) are in agreement with that and illustrate how decoration with zwitterionic species may efficiently screen the cationic charges of parent **CD-0**. Polyelectrolyte titration experiments and determination of the Q_{ek} values enable a better view inside the 3D charge distribution within the NPs (not strictly focused on the charges displayed at the slipping plane) (Weiss et al., 2021) and thus enable a better assessment of those cationic charges available for complexation with anions (*e.g.*, DNA). The Q_{ek} values recorded for all the zwitterionic CDs are less than that for **CD-0**. This reveal that the decorations impede anionic polyelectrolyte from accessing more internal ammonium groups as was the case with **CD-0**. This especially holds for **CD-5** and even more for **CD-6** which has a ζ-potential value close to zero. Besides, no correlation appears when considering the grafting ratios of the CDs and the ζ-potential or Q_{ek} associated values. This is consistent with the previous observations and is the most obvious in the series of CDs bearing the same zwitterionic groups, **CD-6, CD-7**, and **CD-9**, which all are decorated with a sulfobetaine moiety. This suggests that the linker between the NPs and the zwitterionic modules plays an important role in the presentation of zwitterions at the surface of the NPs and, consequently, the expression of stealth properties. With respect to **CD-10**, the larger hydrodynamic diameter accounts for aggregation that might be a consequence of hydrophobic interactions between NPs, possibly due to the presence of hydrophobic methyl thioester functional groups. With the same idea, the sharp increase in the ζ-potential value, when compared to **CD-0**, could be interpreted as the result of exacerbated hydrophobic interactions leading to a better exposition of the cationic groups towards the aqueous environment at the periphery of the NPs. This had reduced impact on the density of cationic charges of theses NPs. Considering the optical properties of the CDs, they are not altered by the presence of grafting groups at their surface. All the NPs described herein thus show identical photophysical parameters that are quite close to those commonly reported for CDs with a typically strong absorption in the UV range and dominant emission in the blue range. Their maximal absorbance is thus observed at 350 nm, and their fluorescence excitation and emission wavelengths are 360 and 450 nm, respectively.

3.2. *Nanoparticle-mucus interactions*

Assessing the interactions between particles and mucus components is critical to defining the ability of these particles to diffuse through and cross the mucus layer. The absence of interactions is generally considered an imperative condition for an effective mucus-penetrating nanoparticulate system. (Kim et al., 2016) To evaluate the interactions between mucus and **CD-0** to **CD-10**, or the dotoplexes made thereof, we used mucin from porcine stomach (PGM) as a simplified mucus model. First, we conducted turbidimetric measurements, mucin aggregation upon interaction with NP translating into increased turbidity. The turbidity of mucin solutions to which CDs were added was measured at 600 nm (Fig. 2A). Sharp increase in the absorbance (ΔA) was observed for **CD-0** what was expected since positively charged NPs are notoriously

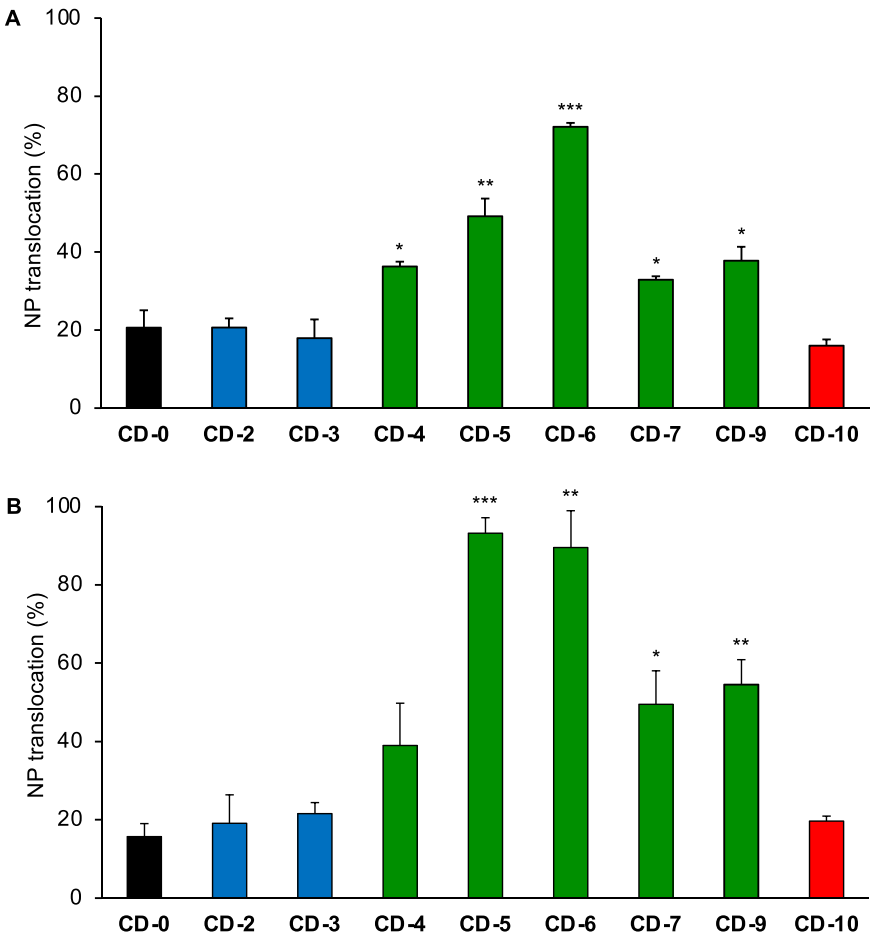

Fig. 3. Transport of CDs (**A**) and CD/DNA complexes (**B**) through a mucus layer over a 5-h incubation period at 37 °C. CD/DNA ratios (w/w) assayed in these experiments were those for which transfection efficiency was optimum in the Calu-3 ALI model (*vide infra*). The amount of NPs that crossed the barrier is expressed as the percentage of the total amount of material deposited onto the mucus layer in the apical compartment. Results are the mean ± SD of $n = 3$–4 experiments. Statistical differences when compared to **CD-0** were determined by Student's *t*-test: $p < 0.05$ (*), $p < 0.01$ (**), and $p < 0.001$ (***).

known to induce mucin aggregation through electrostatic interactions. (Chen et al., 2010) The results obtained with PEGylated NPs, **CD-2** and **CD-3**, were intriguing as these NPs increased aggregation even more than **CD-0**. This however may be tentatively explained by the theories of polymer-polymer adhesion, especially the diffusion theory proposed by Voyutskii. (Voyutskii, 1963) This theory refers to interpenetration of the polymer chains in the interfacial region promoting an adhesive process. In the case of **CD-2** and **CD-3**, aggregation resulting from electrostatic interactions would be thus magnified by entanglement of PEG chains with mucin fibers. Zwitterion-coated CDs turned out to be much more muco-inert candidates in the turbidimetric assay, since only a slight increase in absorbance of the mucin solution was observed, whatever the ζ-potential of the NPs added. For its part, **CD-10** equipped with intrinsic mucolytic properties significantly promoted mucin aggregation, although slightly less than **CD-0**. This was not unexpected, however, as the mucus model used in these experiments is based on purified mucin. Thus, it lacks the enzyme activity that could be responsible for thioester hydrolysis and the subsequent release of methyl mercaptan and mucolytic effect. The same type of experiments has been conducted with dotoplexes (Fig. 2B). Although complexation of CDs with DNA yields NPs with partial neutralization of the positive charges (Table S1), results of the turbidimetric measurements with dotoplexes differ little from those with bare CDs. There are two exceptions to this, and DNA complexes with **CD-2** and **CD-10** performed nearly as well as dotoplexes prepared from zwitterionic CDs, revealing lower interaction with the mucin network. A thorough interpretation of these data is challenging because the complexation of NPs with nucleic acid changes not only their charge but also their size (Table S1), and size is a determining factor in the ability to interact with multiple mucin strands at once and cause aggregation.

The mucus-penetrating ability of the different NPs was then explored using a translocation assay. CDs or the corresponding dotoplexes were deposited onto a mucin layer installed on the semi-permeable membrane of an insert. Thanks to the intrinsic photoluminescence properties of CDs, transport of the latter through the membrane-supported mucus barrier was straightforwardly assessed by measuring fluorescence in the basolateral compartment. Measurements were performed 5 h after deposition of the NPs onto the mucus blanket. This time was selected as it allows a good detection of the CD fluorescence while allowing the highlighting of diffusion differences between CDs. The results showed that only a small fraction of **CD-0** (20 %) could diffuse through the mucus layer during the incubation period (Fig. 3A). PEGylated NPs did not perform better but CDs coated with zwitterionic groups revealed much more efficient with a diffusion improved by a factor of 1.6 to 3.5 when compared to **CD-0**, the prize going to **CD-6** that could complete 72 % translocation into the basolateral compartment. This tendency was even more pronounced with dotoplexes which cationic charges (*i.e.*, potential binding sites to negatively charged mucins) are partly neutralized by phosphates in the DNA backbone (Fig. 3B). Dotoplexes prepared from **CD-5** and **CD-6** did thus reach the lower compartment of the insert at 93 and 84 %, respectively. In this test too, **CD-10** did not really differentiate from parent **CD-0**. Once again, a detailed interpretation of the data based on the size and charge of the NPs is rather intricate.

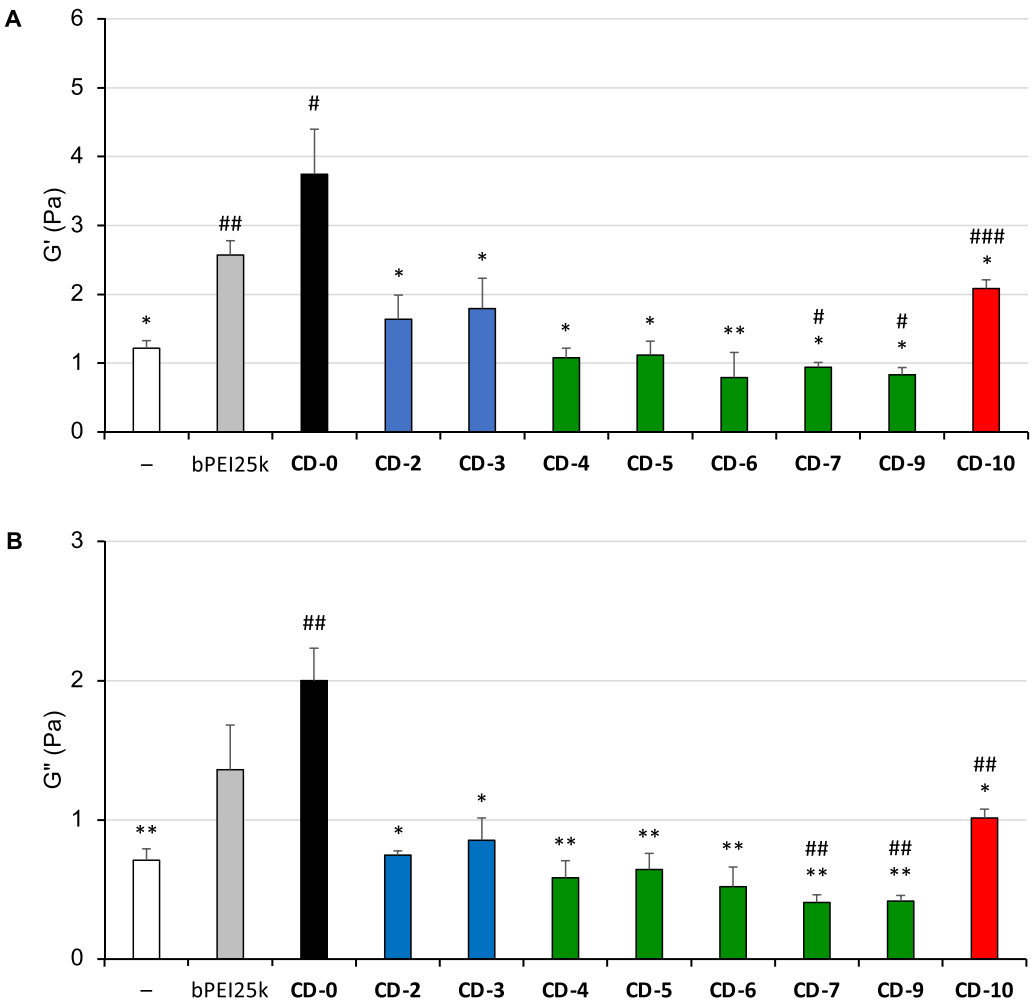

Fig. 4. Variations of the macro-rheological elastic modulus G' (**A**) and loss modulus G" (**B**) of the mucus model in the presence of the cationic gene carriers, bPEI25k and CDs (frequency: 0.1 Hz, strain amplitude: 5 %). (–) corresponds to data for untreated mucus. Statistical differences when compared to **CD-0** (*) or untreated cells (#) were determined by Student's t-test: $p < 0.05$ (one symbol), $p < 0.01$ (two symbols), $p < 0.001$ (three symbols).

At the macroscopic level, mucus is a complex non-Newtonian, thixotropic gel. According to shear stress, it acts as an elastic solid or a viscous liquid. The rheological properties of mucus thus differ as a function of shear stress, time rate of shearing and length scale. (Lai et al., 2009) In order to investigate how the rheological behavior of the mucus 3D network may be affected by the cationic NPs, we conducted macro-rheological studies and quantified variations of the viscoelastic properties of the mucin-based hydrogel provoked by CDs. Storage (G') and loss (G") moduli of the neat hydrogel (100 mg/mL PGM) or hydrogel mixed with **CD-1** to **CD-10** (5 mg/mL) were determined with strain amplitude of 5 %, and bPEI25k was introduced for comparison purpose (Fig. S1). Summarizing these data by focusing to G' and G" at frequency of 0.1 Hz, showed that **CD-0** significantly enhanced viscoelasticity of the hydrogel with G' increasing from 1.22 to 3.74 Pa (Fig. 4A). This effect was even stronger than that produced by bPEI25k (2.57 Pa). Decoration of **CD-0** with PEG reduced the G' value close to that measured for the untreated hydrogel which might seem surprising given the results obtained in the aggregation and translocation assays. However, it is important to keep in mind that these rheological studies give information at the macro scale (bulk fluid) whereas the two other techniques provide data at the micro scale (bimolecular interactions). **CD-0** grafting with zwitterionic species allowed full preservation of rheological properties of the mucus model with **CD-6, CD-7**, and **CD-9** that were even able to significantly reduce elasticity of the gel. With regard to **CD-10**, intermediate results were obtained and G' was reduced by 45 % when compared to **CD-0**. A similar trend was observed when looking at the variations of the loss modulus G" (Fig. 4B). These results revealed that cationic NPs or polymers significantly alter mechanical properties of mucus by increasing its viscoelasticity. However, adequate decoration of these NPs may allow preservation of the original rheological properties of the hydrogel or even reduce its viscoelasticity as was the case with **CD-6, CD-7**, and **CD-9**.

Qualitatively, the results obtained in the translocation assay are consistent with those from the turbidimetric measurements, *i.e.*, we observe decreased interactions within mucins and NPs when they are coated with zwitterionic groups, but not when decorated with PEG chains, rather the opposite. This outcome can be rationalized considering PEG-mucin entanglement may propagate mucoadhesion, as predicted by polymer-polymer adhesion theories. Depending on the length, density, and surface conformation of PEG chains, the coated NPs can display either mucopenetration or mocoadhesion properties. Mucopenetration is most commonly obtained when dense coverage of NPs with short PEG chains (MW 2-5 kDa) is achieved, (Wang et al., 2008) while longer polymer chains and lower PEG coverage result in mucoadhesive NPs. (Yoncheva et al., 2005) This however was essentially concluded from experiments realized with dense polystyrene (PS) NPs. In the case of PEGylated PS nanobeads, it is assumed that PEG chains are directly anchored onto the solid core of the NPs and thus do not have the mobility of a free polymer chain. Such a picture might not apply to the herein described PEI-decorated CDs that were *ex-post* functionalized.

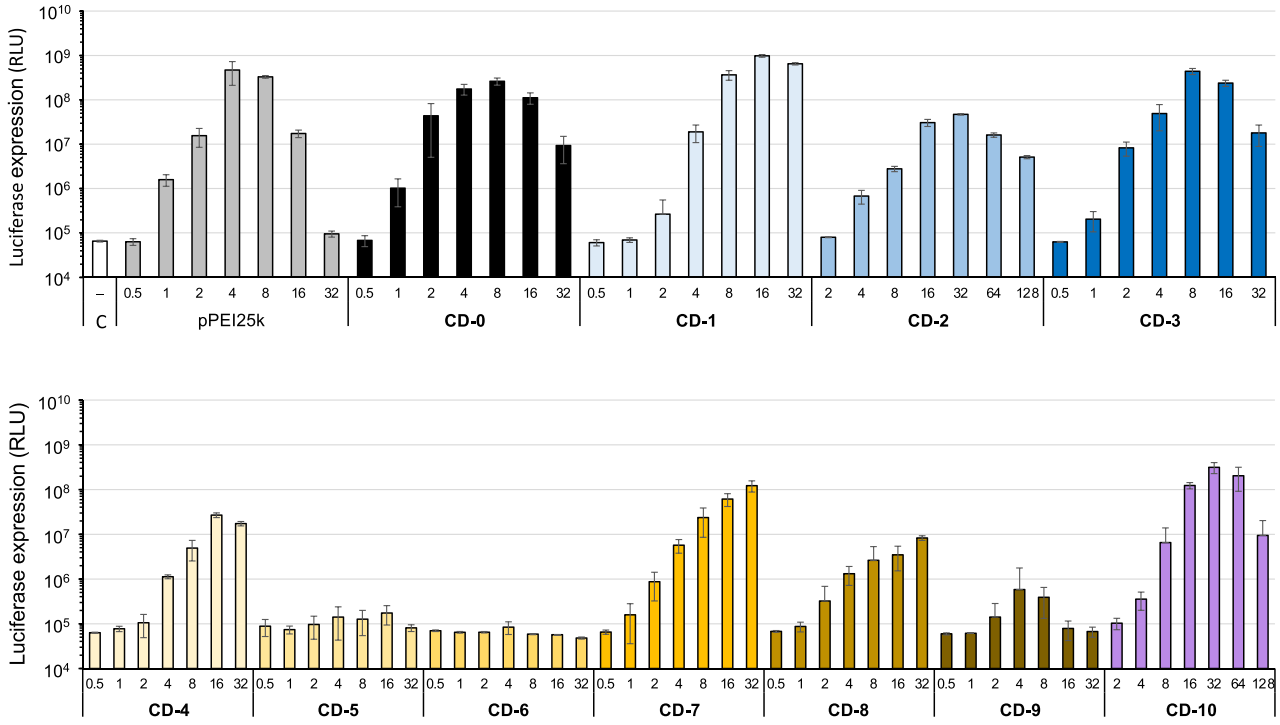

Fig. 5. Expression of luciferase in A549 cells treated with pCMV-GLuc complexed with **CD-0** to **CD-10**, or with bPEI25k (positive control) at various carrier/DNA weight ratios (0.5 to 128). Control (C) refers to basal bioluminescence measured in untreated cells. Data shown are representative of a triplicate determination (mean ± SD).

Consequently, PEG is hanging on flexible PEI chains and may more easily diffuse and spread around and become tangled with mucin fibers. Quantitatively, the translocation assay allows determination of permeation of CDs and dotoplexes through the mucus gel and, in contrast with turbidimetric measurements, highlights effects of the complexation of CDs with DNA. With respect to macro-rheological measurements, they showed that decoration of NPs with PEG did significantly impact viscoelasticity of the gel as was the case with CDs functionalized with

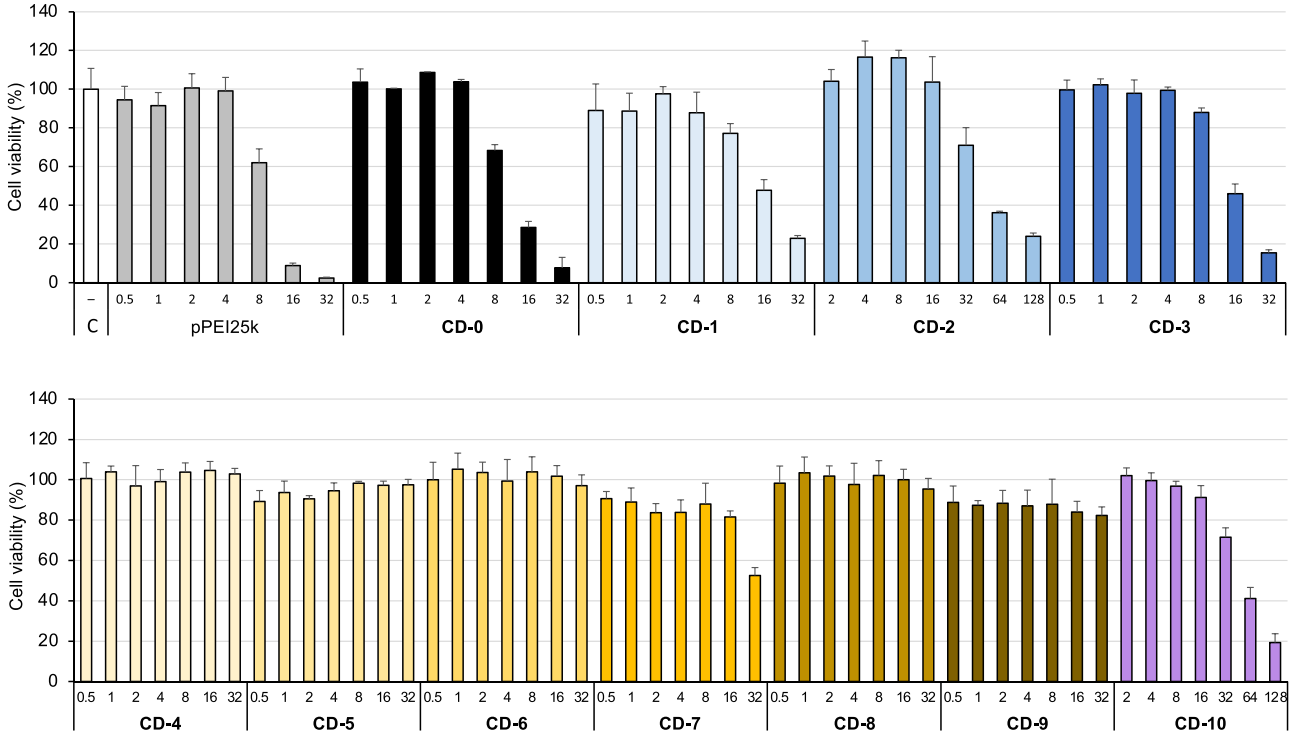

Fig. 6. Cytotoxicity of the various CD/pDNA complexes after incubation with A549 cells for 24 h as measured by the MTT assay. Results are expressed as the percentage of the absorbance of treated cells relative to that of untreated cells. Data shown are representative of triplicate determinations (mean ± SD).

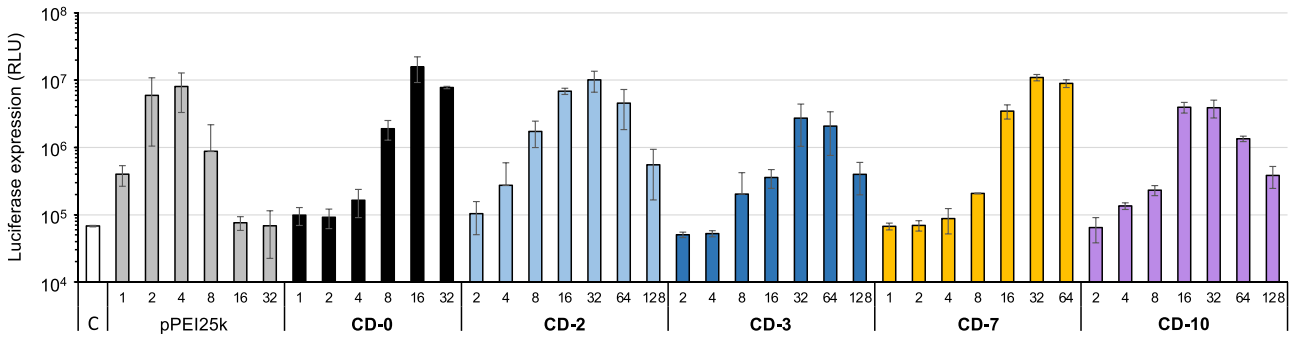

Fig. 7. Expression of luciferase in plate cultures of Calu-3 cells treated with pCMV-GLuc complexed with CDs, and with bPEI25k as positive control. Complexes were prepared at various carrier/DNA weight ratios (1 to 128). Control (C) refers to basal bioluminescence measured in untreated cells. Data shown are representative of a triplicate determination (mean ± SD).

zwitterions. The G' and G" values were thus decreased by a factor of 2–5, and 2–7, respectively, the larger effect being observed with **CD-7**.

3.3. DNA delivery

We next investigated whether the engineered CDs could improve transgene expression in cultured cells. First, we assessed complex formation between CDs and DNA. For that, DNA retardation assays were performed using agarose gel electrophoresis. The results showed that all CDs have high capability to bind DNA, and full plasmid complexation was observed at CD/DNA ratio (w/w) below 0.6-1 (Fig. S2). One exception was found with **CD-6** for which a higher mass ratio (> 16) was required for full DNA complexation. These results pretty well correlate with Q_{ek} values ($r = 0.91$), except for **CD-4** and **CD-6** (Table 1). Then, transfection efficiency of dotoplexes was assessed by delivering a plasmid DNA expressing *Gaussia princeps* luciferase (pCMV-GLuc) into the lung epithelial cells A549 and Calu-3 that were cultured either in plates or on inserts at the ALI. Bioluminescence measurements were performed to straightforwardly quantify transgene expression. In A549 cells cultured in plates, parent **CD-0** was found as effective at delivering pCMV-GLuc as bPEI25k, a gold standard in gene delivery that was used as a positive control (Fig. 5). Though PEG decoration of NPs generally has an adverse effect on cell uptake *in vitro*, PEGylation of **CD-0** did not much impact gene delivery properties of the resulting CDs, except for **CD-2** for which transfection efficiency decreased by *ca.* an order of magnitude. Thus, **CD-1** and **CD-3** did perform as well or better than **CD-0**, and the CD/DNA ratio (w/w) for maximum transfection efficiency was only slightly increased with **CD-1**, when compared to **CD-0**, and did not significantly change with **CD-3**. The transfection efficiency of PEGylated CDs can be tentatively correlated with the size of the dotoplexes (Table S1). This is based on the premise that larger complexes sediment more readily on cells and are more efficiently internalized. However, it is evident that a direct parallel cannot be drawn between dotoplex internalization and transgene expression, as the latter is still dependent on the intracellular processing of the transfection particles, including endosomal escape, nucleic acid decomplexation, and import into the nucleus. Regarding to zwitterion-decorated CDs, mixed results were obtained. While **CD-7** revealed as a highly potent carrier for intracellular plasmid DNA delivery, **CD-4** and **CD-8** proved less powerful, and **CD-5, CD-6**, and **CD-9** were totally ineffective. This phenomenon could be attributed to the higher ζ potential of dotoplexes based on **CD-7** and **CD-8** (+25.1 ± 0.1 and +20.9 ± 0.6 mV, resp.). In all cases, transgene expression with zwitterion-decorated CDs was observed at higher CD/DNA ratios (w/w) when compared to **CD-0. CD-10** resulting from functionalization of **CD-0** with thioester-containing reagent **10** did perform similarly to the parent CDs and no significant difference in transfection efficiency was observed except that maximum activity was obtained at higher CD/DNA ratio. Even more so than in the previous tests, these results are difficult to interpret on the basis of dotoplex size and charge, as the intracellular processing of the transfection NPs can be radically altered depending on the nature of the decorations displayed at their periphery.

In order to address the safety issue, viability of A549 cells exposed to dotoplexes prepared with increasing amounts of CDs was assessed using the MTT assay (Fig. 6). The results revealed that those CDs that were not (**CD-5, CD-6**, and **CD-9**) or only poorly (**CD-4** and **CD-8**) active as gene delivery carriers did not elicit significant toxicity. At the higher concentration tested, the viability of cells still was higher than 80–90 %. For those CDs that were capable of inducing strong transfection response, associated cytotoxicity was invariably found at the higher carrier concentrations, as was also observed for bPEI25k. In all cases however, more than 70 % mitochondrial activity was preserved at the CD concentration for optimal gene delivery, suggesting that the CDs have no adverse effect on A549 cells within the application limit.

We next investigated the potential of CDs to deliver DNA into cells covered by a mucus layer to better mimic the situation met by the transfection particles when locally administered into the lung. For that we used a previously developed *in vitro* model based on the Calu-3 cell line. (Sonntag et al., 2022) Calu-3 cells are mucus-producing submucosal-gland carcinoma cells. The amount of mucus they produce can be greatly increased when they are cultured at the ALI on inserts. The thickness of the mucus layer thus formed increases with time of ALI culture, and after 7 d reaches *ca.* 10–12 μm as was assessed by confocal laser scanning microscopy. (Sonntag et al., 2022) As Calu-3 cells are harder to transfect than A549 cells, (Pierrat et al., 2016) a preliminary evaluation of dotoplexes was conducted in conventional plate cultures. As a good rule of thumb, transgene expression in plate cultures of Calu-3 cells was about one hundred times lower than in plate cultures of A549 cells (Fig. 7). Consequently, carriers which did not performed well in A549 cells failed to induce significant transgene expression in Calu-3 cells (**CD-4, CD-5, CD-6, CD-8**, and **CD-9**, data not shown). **CD-0, CD-2**, and **CD-7** gave similar results whereas **CD-3** and **CD-10** were a little less efficient. Positive control bPEI25k gave intermediate results. These CDs were thus retained for further evaluation in the Calu-3 ALI model. Only formulations with carrier/DNA ratio (w/w) leading to maximum transfection, according to the results obtained in Calu-3 plate cultures, were assayed, and transfection efficiency was assessed 24 h or 72 h after dotoplex addition onto inserts. At the first time point, virtually no transfection was measured revealing considerable retention effect of mucus on transfection particles. We hypothesized that *Gaussia p.* luciferase secreted by cells could be possibly retained in the mucus meshes leading to under evaluating the concentration of transgene product secreted by cells. To avoid this difficulty, supernatant and the mucus layer were gently removed from the inserts 24 h after dotoplex deposition and cells were washed with culture medium before another incubation period of 48 h, followed by a second assessment of transgene

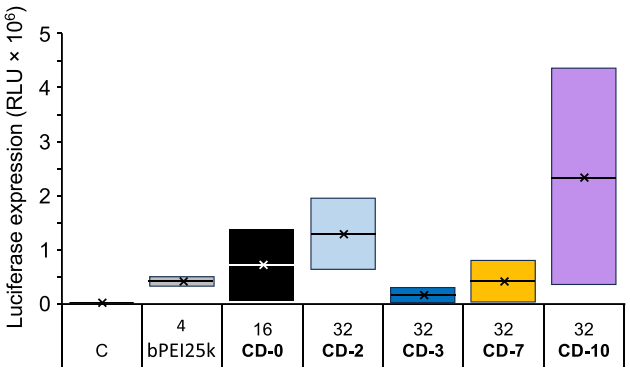

Fig. 8. Transfection efficiency of the CDs in the Calu-3 ALI model. Cells were treated with pCMV-GLuc complexed with CDs, or with bPEI25k as positive control. Carrier/DNA weight ratios (4 to 32) are those found optimal for transfection of Calu-3 cells cultured in plates (cf. Fig. 7). Transgene expression was assessed 72 h after dotoplex deposition onto cells (see in the body text). Control (C) refers to basal bioluminescence measured in untreated cells. Data shown are representative of a duplicate determination.

expression (Fig. 8). Whereas parent **CD-0** yielded slightly better performances than bPEI25k, its decoration with PEG chains (**CD-2**) and thioesters (**CD-10**) increased transfection efficiency approximately by a factor 1.7 and 3.1, respectively. Heavily PEGylated **CD-3** scored below less densely PEGylated **CD-2**. This trend was already observed in Calu-3 plate cultures and tends to be stronger in the ALI model. This is consistent with results obtained in the previous turbidimetry measurements where **CD-3**/DNA dotoplexes did interact more tightly with mucins. That transfection is impaired by interactions between dotoplexes and mucus or because of lower cell uptake or endosomal escape remains to be determined. However, opposite transfection results obtained in the A549 cell model do suggest a key role of mucus. Zwitterionic decorations on CDs did not help improve transfection rate in the Calu-3 ALI model, rather the opposite, as observed with **CD-7**. On the contrary, NP decoration with thioesters significantly improved transfection efficiency and **CD-10** outperformed parent **CD-0**. Hydrolytic enzymes in the cell mucus more likely are responsible for hydrolysis of the thioester decorations and release of methyl mercaptan in the bulk biopolymer. Reduction of disulfide bridges by methyl mercaptan would thus result in a decrease in the viscoelasticity of mucus and a higher diffusion rate of the transfection particles towards the underlying cells. This however is an interpretation and experimental validation would require complementary turbidimetry and translocation measurements, *e.g.*, with a more sophisticated mucus model incorporating enzymes with hydrolytic activity.

Considering cell viability, it remained above 70 % in the Calu-3 plate cultures, even at the higher dose of dotoplexes deposited on cells (Fig. S3). This observation differs from that made in the A549 cell line and is likely explained by the lower amount of dotoplexes having reached the mucus-secreting cells. Though mucus secreted by Calu-3 cells when cultured in plates for a 24-h period before dotoplex deposition does not yet form a fully protective barrier, it seems that it is already powerful enough to trap a significant amount of transfection NPs. Consequently, less are internalized by cells which viability is thus better preserved. In the Calu-3 ALI model, cell viability was assessed 72 h post incubation and was found significantly decreased after treatment with bPEI25k/DNA polyplexes, not exceeding 60 % in this case (Fig. 9). Generally, dotoplexes did better preserved cells and **CD-10** which has proven most effective to transfect cells in the ALI model was found perfectly tolerated, with cell viability as high as 91 %.

4. Conclusion

In this work, we asked how the surface decoration of cationic CDs can promote their penetration and diffusion into mucin gels and thus improve their capacity to deliver nucleic acid into lung epithelial cells. We have shown that decoration of cationic CDs can significantly modify their properties, reducing interaction with mucus, and allowing faster diffusion through the biopolymer, with no increase in viscoelasticity of the bio gel. This, *in fine*, was expected to improve transfection efficiency of cells lined with mucus. However, it comes out that fully muco-inert NPs (*i.e.*, **CD-5** or **CD-6**) may not be ideally suited for such purpose. Indeed, if NPs do not interact with mucus and freely diffuse, they may also not interact with membrane of epithelial cells (resulting in poor cell uptake) or endosome membrane (resulting in sequestration and degradation of the nucleic acid cargo in endo-lysosomes), yielding low performances in terms of transgene expression. Herein, we showed that decoration of cationic CDs with PEG, but not with zwitterionic species, may enhance intracellular nucleic acid delivery and transfection efficiency. PEG however is a double-edged sword as it may provide mucoinert or mucoadhesive properties to NPs, depending on the PEG chain length and grafting density. The "PEG outcome" can be rationalized considering entanglement of mucin fibers and PEG chains as predicted by polymer-polymer adhesion theories. More substantial transfection efficiency enhancement was obtained with CDs that were decorated with methyl thioester groups so as to equip the NPs with intrinsic mucolytic activity through the release of methyl mercaptan. Further development of this new strategy for gene delivery to the lung

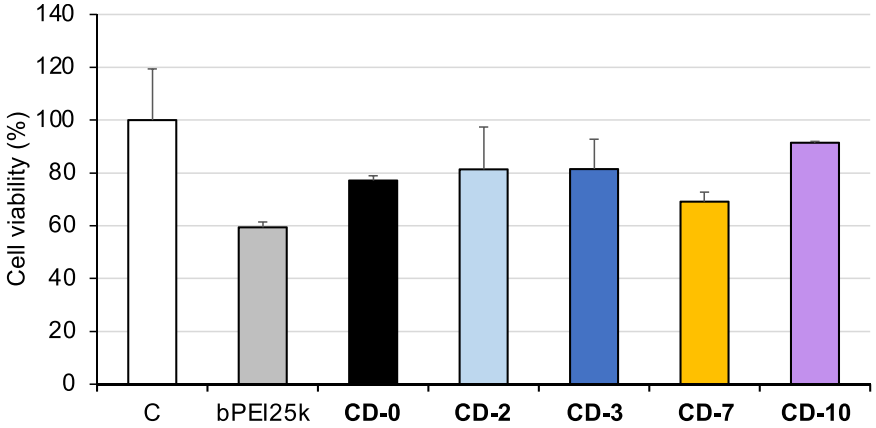

Fig. 9. Cytotoxicity of the various CD/pDNA complexes after incubation with Calu-3 cultured at ALI for 7 d. Cell viability was assessed by the MTT assay 72 h after deposition of the complexes on the cells. Results are expressed as the percentage of the absorbance of treated cells relative to that of untreated cells. Data shown are representative of duplicate determinations (mean ± SD).

and other mucosal tissues is currently underway.

Ethical approval statement

All experiments were conducted in an ethical and responsible manner and are in full compliance with all relevant codes of experimentation and legislation. This study was conducted exclusively using in-vitro cell culture methods. No animal or human subjects were involved in this research, and thus, no ethical approval was required.

All authors declare that they have no known competing financial interests or personal relationships that could have appeared to influence the work reported in this paper.

Funding

This work has recieved financial support from « Blanche pour Vaincre la Mucoviscidose » and Association Vaincre la Mucoviscidose (VLM 202,109-VFS).

CRediT authorship contribution statement

Samuel Arca: Methodology, Investigation, Formal analysis. **Françoise Pons:** Writing – review & editing, Validation, Conceptualization. **Luc Lebeau:** Writing – review & editing, Writing – original draft, Visualization, Validation, Supervision, Project administration, Funding acquisition, Conceptualization.

Declaration of competing interest

All authors declare that they have no known competing financial interests or personal relationships that could have appeared to influence the work reported in this paper.

Acknowledgements

The authors wish to thank Fanny Burger, Julia Fath and Anaïs Roos for technical assistance.

Supplementary materials

Supplementary material associated with this article can be found, in the online version, at doi:10.1016/j.ejps.2025.107222.

Data availability

Data will be made available on request.

References

Agu, R.U., Ugwoke, M.I., Armand, M., Kinget, R., Verbeke, N., 2001. The lung as a route for systemic delivery of therapeutic proteins and peptides. Respir. Res. 2, 198–209. https://doi.org/10.1186/rr58.

Balsamo, R., Lanata, L., Egan, C.G., 2010. Mucoactive drugs. Eur. Respir. Rev. 19, 127–133. https://doi.org/10.1183/09059180.00003510.

Bansil, R., Turner, B.S., 2018. The biology of mucus: composition, synthesis and organization. Adv. Drug Deliv. Rev. 124, 3–15. https://doi.org/10.1016/j.addr.2017.09.023.

Biswal, M.R., Bhatia, S., 2021. Carbon dot nanoparticles: exploring the potential use for gene delivery in ophthalmic diseases. Nanomaterials 11, 935. https://doi.org/10.3390/nano11040935.

Broughton-Head, V.J., Smith, J.R., Shur, J., Shute, J.K., 2007. Actin limits enhancement of nanoparticle diffusion through cystic fibrosis sputum by mucolytics. Pulm. Pharmacol. Ther. 20, 708–717. https://doi.org/10.1016/j.pupt.2006.08.008.

Chen, E.Y.T., Wang, Y.C., Chen, C.S., Chin, W.C., 2010. Functionalized positive nanoparticles reduce mucin swelling and dispersion. Plos One 5, e15434. https://doi.org/10.1371/journal.pone.0015434.

Claudel, M., Fan, J.H., Rapp, M., Pons, F., Lebeau, L., 2019. Influence of carbonization conditions on luminescence and gene delivery properties of nitrogen-doped carbon dots. RSC Adv. 9, 3493–3502. https://doi.org/10.1039/c8ra09651a.

Cone, R.A., 2009. Barrier properties of mucus. Adv. Drug Deliv. Rev. 61, 75–85. https://doi.org/10.1016/j.addr.2008.09.008.

Dasgupta, B., King, M., 1996. Reduction in viscoelasticity in cystic fibrosis sputum in vitro using combined treatment with nacystelyn and rhDNase. Pediatr. Pulmonol. 22, 161–166. https://doi.org/10.1002/(sici)1099-0496(199609)22:3<161::Aid−ppul4>3.3.Co;2-3.

Ensign, L.M., Schneider, C., Suk, J.S., Cone, R., Hanes, J., 2012. Mucus penetrating nanoparticles: biophysical tool and method of drug and gene delivery. Adv. Mater. 24, 3887–3894. https://doi.org/10.1002/adma.201201800.

Fahy, J.V., Dickey, B.F., 2010. Airway mucus function and dysfunction. New Engl. J. Med. 363, 2233–2247. https://doi.org/10.1056/NEJMra0910061.

Ferrari, S., Kitson, C., Farley, R., Steel, R., Marriott, C., Parkins, D.A., Scarpa, M., Wainwright, B., Evans, M.J., Colledge, W.H., et al., 2001. Mucus altering agents as adjuncts for nonviral gene transfer to airway epithelium. Gene Ther. 8, 1380–1386. https://doi.org/10.1038/sj.gt.3301525.

Forest, V., Pourchez, J., 2022. Nano-delivery to the lung- by inhalation or other routes and why nano when micro is largely sufficient? Adv. Drug Deliv. Rev. 183, e114173. https://doi.org/10.1016/j.addr.2022.114173.

Ghadiri, M., Young, P.M., Traini, D., 2019. Strategies to enhance drug absorption via nasal and pulmonary routes. Pharmaceutics 11, 20. https://doi.org/10.3390/pharmaceutics11030113.

Gill, S., Lobenberg, R., Ku, T., Azarmi, S., Roa, W., Prenner, E.J., 2007. Nanoparticles: characteristics, mechanisms of action, and toxicity in pulmonary drug delivery. A review. J. Biomed. Nanotechnol. 3, 107–119. https://doi.org/10.1166/jbn.2007.015.

Guo, Y., Bera, H., Shi, C., Zhang, L., Cun, D., Yang, M., 2021. Pharmaceutical strategies to extend pulmonary exposure of inhaled medicines. Acta Pharm. Sinica B 11, 2565–2584. https://doi.org/10.1016/j.apsb.2021.05.015.

Henry, C.E., Wang, Y.Y., Yang, Q., Hoang, T., Chattopadhyay, S., Hoen, T., Ensign, L.M., Nunn, K.L., Schroeder, H., McCallen, J., et al., 2016. Anti-PEG antibodies alter the mobility and biodistribution of densely PEGylated nanoparticles in mucus. Acta Biomater. 43, 61–70. https://doi.org/10.1016/j.actbio.2016.07.019.

Huckaby, J.T., Lai, S.K., 2017. PEGylation for enhancing nanoparticle diffusion in mucus. Adv. Drug Deliv. Rev. 124, 125–139. https://doi.org/10.1016/j.addr.2017.08.010.

Kaurav, H., Verma, D., Bansal, A., Kapoor, D.N., Sheth, S., 2023. Progress in drug delivery and diagnostic applications of carbon dots: a systematic review. Front. Chem. 11, 1227843. https://doi.org/10.3389/fchem.2023.1227843.

Kim, A.J., Boylan, N.J., Suk, J.S., Hwangbo, M., Yu, T., Schuster, B.S., Cebotaru, L., Lesniak, W.G., Oh, J.S., Adstamongkonkul, P., et al., 2013. Use of single-site-functionalized PEG dendrons to prepare gene vectors that penetrate Human mucus barriers. Angew. Chem. Int. Ed. 52, 3985–3988. https://doi.org/10.1002/anie.201208556.

Kim, N., Duncan, G.A., Hanes, J., Suk, J.S., 2016. Barriers to inhaled gene therapy of obstructive lung diseases: a review. J. Control. Release 240, 465–488. https://doi.org/10.1016/j.jconrel.2016.05.031.

Knowles, M.R., Boucher, R.C., 2002. Mucus clearance as a primary innate defense mechanism for mammalian airways. J. Clin. Invest. 109, 571–577. https://doi.org/10.1172/jci200215217.

Kolb, M., Martin, G., Medina, M., Ask, K., Gauldie, J., 2006. Gene therapy for pulmonary diseases. Chest 130, 879–884. https://doi.org/10.1378/chest.130.3.879.

Kushwah, R., Oliver, J.R., Cao, H., Hu, J., 2007. Nacystelyn enhances adenoviral vector-mediated gene delivery to mouse airways. Gene Ther. 14, 1243–1248. https://doi.org/10.1038/sj.gt.3302968.

Laffleur, F., Bernkop-Schnurch, A., 2013. Strategies for improving mucosal drug delivery. Nanomedicine 8, 2061–2075. https://doi.org/10.2217/nnm.13.178.

Laffleur, F., Hintzen, F., Shahnaz, G., Rahmat, D., Leithner, K., Bernkop-Schnurch, A., 2014. Development and in vitro evaluation of slippery nanoparticles for enhanced diffusion through native mucus. Nanomedicine 9, 387–396. https://doi.org/10.2217/nnm.13.26.

Lai, S.K., Wang, Y.Y., Hanes, J., 2009. Mucus-penetrating nanoparticles for drug and gene delivery to mucosal tissues. Adv. Drug Deliv. Rev. 61, 158–171. https://doi.org/10.1016/j.addr.2008.11.002.

Li, Y., Liu, R.Y., Shi, Y.J., Zhang, Z.Z., Zhang, X., 2015. Zwitterionic poly (carboxybetaine)-based cationic liposomes for effective delivery of small interfering RNA therapeutics without accelerated blood clearance phenomenon. Theranostics 5, 583–596. https://doi.org/10.7150/thno.11234.

Lieleg, O., Ribbeck, K., 2011. Biological hydrogels as selective diffusion barriers. Trends Cell Biol. 21, 543–551. https://doi.org/10.1016/j.tcb.2011.06.002.

Lim, S.Y., Shen, W., Gao, Z.Q., 2015. Carbon quantum dots and their applications. Chem. Soc. Rev. 44, 362–381. https://doi.org/10.1039/c4cs00269e.

Luo, M.X., Hua, S., Shang, Q.Y., 2021. Application of nanotechnology in drug delivery systems for respiratory diseases. Mol. Med. Rep. 23, e325. https://doi.org/10.3892/mmr.2021.11964.

Majima, Y., Inagaki, M., Hirata, K., Takeuchi, K., Morishita, A., Sakakura, Y., 1988. The effect of an orally-administered proteolytic-enzyme on the elasticity and viscosity of nasal mucus. Arch. Otorhinolaryngol. 244, 355–359. https://doi.org/10.1007/bf00497464.

Mansour, H.M., Rhee, Y.S., Wu, X., 2009. Nanomedicine in pulmonary delivery. Int. J. Nanomed. 4, 299–319. https://doi.org/10.2147/ijn.s4937.

Mansuriya, B.D., Altintas, Z., 2021. Carbon dots: classification, properties, synthesis, characterization, and applications in health care - an updated review (2018-2021). Nanomaterials 11, e2525. https://doi.org/10.3390/nano11102525.

Matthews, L.W., Spector, S., Lemm, J., Potter, J.L., 1963. Studies on pulmonary secretions. I. The over-all chemical composition of pulmonary secretions from patients with cystic fibrosis, bronchiectasis, and laryngectomy. Am. Rev. Respir. Disease 88, 199–204. https://doi.org/10.1164/arrd.1963.88.2.199.

Neuberg, P., Kichler, A., 2014. Recent developments in nucleic acid delivery with polyethylenimines. In: Huang, L., Liu, D., Wagner, E. (Eds.), Advances in Genetics, Advances in Genetics, 88. Academic Press, pp. 263–288.

Othman, H.O., Anwer, E.T., Ali, D.S., Hassan, R.O., Mahmood, E.E., Ahmed, R.A., Muhammad, R.F., Smaoui, S., 2024. Recent advances in carbon quantum dots for gene delivery: a comprehensive review. J. Cell. Physiol. 239, e31236. https://doi.org/10.1002/jcp.31236.

Peng, H., Ji, W.H., Zhao, R.C., Lu, Z.G., Yang, J., Li, Y., Zhang, X., 2020. pH-sensitive zwitterionic polycarboxybetaine as a potential non-viral vector for small interfering RNA delivery. RSC Adv. 10, 45059–45066. https://doi.org/10.1039/d0ra09359a.

Pickles, R.J., 2004. Physical and biological barriers to viral vector-mediated delivery of genes to the airway epithelium. Proc. Am. Thorac. Soc. 1, 302–308. https://doi.org/10.1513/pats.200403-024MS.

Pierrat, P., Casset, A., Didier, P., Kereselidze, D., Lux, M., Pons, F., Lebeau, L., 2016. Cationic DOPC-detergent conjugates for safe and efficient in vitro and in vivo nucleic acid delivery. Chembiochem 17, 1771–1783. https://doi.org/10.1002/cbic.201600302.

Pierrat, P., Wang, R.R., Kereselidze, D., Lux, M., Didier, P., Kichler, A., Pons, F., Lebeau, L., 2015. Efficient in vitro and in vivo pulmonary delivery of nucleic acid by carbon dot-based nanocarriers. Biomaterials 51, 290–302. https://doi.org/10.1016/j.biomaterials.2015.02.017.

Porsio, B., Craparo, E.F., Mauro, N., Giammona, G., Cavallaro, G., 2018. Mucus and cell-penetrating nanoparticles embedded in nano-into-micro formulations for pulmonary delivery of Ivacaftor in patients with cystic fibrosis. ACS Appl. Mater. Interfaces 10, 165–181. https://doi.org/10.1021/acsami.7b14992.

Rau, J.L., 2005. The inhalation of drugs: advantages and problems. Respir. Care 50, 367–382.

Rose, M.C., Voynow, J.A., 2006. Respiratory tract mucin genes and mucin glycoproteins in health and disease. Physiol. Rev. 86, 245–278. https://doi.org/10.1152/physrev.00010.2005.

Schattling, P., Taipaleenmaki, E., Zhang, Y., Stadler, B., 2017. A polymer chemistry point of view on mucoadhesion and mucopenetration. Macromol. Biosci. 17, e1700060. https://doi.org/10.1002/mabi.201700060.

Schuster, B.S., Suk, J.S., Woodworth, G.F., Hanes, J., 2013. Nanoparticle diffusion in respiratory mucus from humans without lung disease. Biomaterials 34, 3439–3446. https://doi.org/10.1016/j.biomaterials.2013.01.064.

Shepherd, E.J., Kitchener, J.A., 1956. The ionization of ethyleneimine and polyethyleneimine. J. Chem. Soc. 2448–2452. https://doi.org/10.1039/JR9560002448.

Shogren, R., Gerken, T.A., Jentoft, N., 1989. Role of glycosylation on the conformation and chain dimensions of O-linked glycoproteins - light-scattering-studies of ovine submaxillary mucin. Biochemistry 28, 5525–5536. https://doi.org/10.1021/bi00439a029.

Sibum, I., Hagedoorn, P., de Boer, A.H., Frijlink, H.W., Grasmeijer, F., 2018. Challenges for pulmonary delivery of high powder doses. Int. J. Pharm. 548, 325–336. https://doi.org/10.1016/j.ijpharm.2018.07.008.

Sonntag, T., Rapp, M., Didier, P., Lebeau, L., Pons, F., Casset, A., 2022. Mucus-producing epithelial models for investigating the activity of gene delivery systems in the lung. Int. J. Pharm. 614, 121423. https://doi.org/10.1016/j.ijpharm.2021.121423.

Suk, J.S., Boylan, N.J., Trehan, K., Tang, B.C., Schneider, C.S., Lin, J.M.G., Boyle, M.P., Zeitlin, P.L., Lai, S.K., Cooper, M.J., et al., 2011. N-acetylcysteine enhances cystic fibrosis sputum penetration and airway gene transfer by highly compacted DNA nanoparticles. Mol. Ther. 19, 1981–1989. https://doi.org/10.1038/mt.2011.160.

Suk, J.S., Lai, S.K., Wang, Y.Y., Ensign, L.M., Zeitlin, P.L., Boyle, M.P., Hanes, J., 2009. The penetration of fresh undiluted sputum expectorated by cystic fibrosis patients by non-adhesive polymer nanoparticles. Biomaterials 30, 2591–2597. https://doi.org/10.1016/j.biomaterials.2008.12.076.

Sun, J., Zeng, F., Jian, H.L., Wu, S.Z., 2013. Conjugation with betaine: a facile and effective approach to significant improvement of gene delivery properties of PEI. Biomacromolecules 14, 728–736. https://doi.org/10.1021/bm301826m.

Taherali, F., Varum, F., Basit, A.W., 2018. A slippery slope: on the origin, role and physiology of mucus. Adv. Drug Deliv. Rev. 124, 16–33. https://doi.org/10.1016/j.addr.2017.10.014.

Thornton, D.J., Rousseau, K., McGuckin, M.A., 2008. Structure and function of the polymeric mucins in airways mucus. Annu. Rev. Physiol. 70, 459–486. https://doi.org/10.1146/annurev.physiol.70.113006.100702.

Uchida, T., Kurita, Y., Koizumi, N., Kubo, M., 1956. Dipole moments and the structures of polyethylene glycols. J. Polymer Sci. 21, 313–322. https://doi.org/10.1002/pol.1956.120219814.

Voyutskii, S.S., 1963. Autohesion and adhesion of high polymers. Polym. Rev. 4, 249–262.

Wang, Y.Y., Lai, S.K., Suk, J.S., Pace, A., Cone, R., Hanes, J., 2008. Addressing the PEG mucoadhesivity paradox to engineer nanoparticles that "slip" through the Human mucus barrier. Angew. Chem. Int. Ed. 47, 9726–9729. https://doi.org/10.1002/anie.200803526.

Watchorn, J., Clasky, A.J., Prakash, G., Johnston, I.A.E., Chen, P.Z., Gu, F.X., 2022. Untangling mucosal drug delivery: engineering, designing, and testing nanoparticles to overcome the mucus barrier. ACS Biomater. Sci. Eng. 8, 1396–1426. https://doi.org/10.1021/acsbiomaterials.2c00047.

Weiss, M., Fan, J.H., Claudel, M., Sonntag, T., Didier, P., Ronzani, C., Lebeau, L., Pons, F., 2021. Density of surface charge is a more predictive factor of the toxicity of cationic carbon nanoparticles than zeta potential. J. Nanobiotechnol. 19 (5). https://doi.org/10.1186/s12951-020-00747-7.

Witten, J., Samad, T., Ribbeck, K., 2018. Selective permeability of mucus barriers. Curr. Opin. Biotech. 52, 124–133. https://doi.org/10.1016/j.copbio.2018.03.010.

World Health Organization. The top 10 causes of death. [accessed on 2024 sept 10; Available from: https://www.who.int/news-room/fact-sheets/detail/the-top-10-causes-of-death].

Wu, L., Shan, W., Zhang, Z., Huang, Y., 2018. Engineering nanomaterials to overcome the mucosal barrier by modulating surface properties. Adv. Drug Deliv. Rev. 124, 150–163. https://doi.org/10.1016/j.addr.2017.10.001.

Xu, X.Y., Ray, R., Gu, Y.L., Ploehn, H.J., Gearheart, L., Raker, K., Scrivens, W.A., 2004. Electrophoretic analysis and purification of fluorescent single-walled carbon nanotube fragments. J. Am. Chem. Soc. 126, 12736–12737. https://doi.org/10.1021/ja040082h.

Yazdani, S., Mozaffarian, M., Pazuki, G., Hadidi, N., Villate-Beitia, I., Zárate, J., Puras, G., Pedraz, J.L., 2024. Carbon-based nanostructures as emerging materials for gene delivery applications. Pharmaceutics 16, 288. https://doi.org/10.3390/pharmaceutics16020288.

Yoncheva, K., Gómez, S., Campanero, M.A., Gamazo, C., Irache, J.M., 2005. Bioadhesive properties of pegylated nanoparticles. Expert Opin. Drug Deliv. 2, 205–218. https://doi.org/10.1517/17425247.2.2.205.

Zhang, W., Shen, J., Liang, J., Ge, C., Zhou, Y., Yin, L., Ji, Y., 2024. Pulmonary RNA interference against acute lung injury mediated by mucus- and cell-penetrating nanocomplexes. Acta Biomater. 177, 332–346. https://doi.org/10.1016/j.actbio.2024.01.032.

Zhu, J., Guo, M., Cui, Y., Meng, Y., Ding, J., Zeng, W., Zhou, W., 2022. Surface coating of pulmonary siRNA delivery vectors enabling mucus penetration, cell targeting, and intracellular radical scavenging for enhanced acute lung injury therapy. ACS Appl. Mater. Interfaces 14, 5090–5100. https://doi.org/10.1021/acsami.1c23069.